Physical Communication 59 (2023) 102120

Contents lists available at ScienceDirect

Physical Communication

journal homepage: www.elsevier.com/locate/phycom

Full length article

Doubly selective channel estimation and equalization based on ICI/ISI mitigation for OQAM-FBMC systems

Ying Wang [a,c], Qiang Guo [a,b], Jianhong Xiang [a,b,*], Yang Liu [c,d]

[a] College of Information and Communication Engineering, Harbin Engineering University, Harbin 150001, China
[b] Key Laboratory of Advanced Ship Communication and Information Technology, Harbin Engineering University, Harbin 150001, China
[c] Sichuan Key Laboratory of Agile Intelligent Computing, Chengdu 610036, China
[d] Southwest China Institute of Electronics Technology, Chengdu 610036, China

ARTICLE INFO

Article history:
Received 5 April 2023
Received in revised form 29 May 2023
Accepted 30 May 2023
Available online 2 June 2023

Keywords:
OQAM-FBMC
Channel estimation
ICI/ISI mitigation
SAOSP algorithm
Suboptimal MMSE equalization

ABSTRACT

Over a doubly selective channel, broadband transmission systems face challenges in channel estimation and equalization. High mobility causes inter-carrier interference (ICI), while multipath transmission induces inter-symbol interference (ISI). In this paper, we present a mitigation method of ICI/ISI for the offset quadrature amplitude-modulated filter bank multi-carrier (OQAM-FBMC) system. It features low inherent imaginary interference (IMI) sensitivity and high efficiency. Specifically, a pilot indices optimization algorithm and a sparse adaptive orthogonal subspace pursuit (SAOSP) algorithm are presented based on the 2-D channel modeling scheme. The guard pilots are first added to mitigate the effect of ICI. Then the index optimization and SAOSP algorithms are applied to achieve a high-accuracy estimation of sparse channel coefficients. In addition, a threshold judgment suboptimal minimum mean square error (MMSE) equalization method is presented based on the variability of the interference power. The method uses normalized interference power thresholds to estimate the ISI dimension and reduce the equalization data, thus mitigating the effect of ISI and achieving efficient equalization. To verify the above methods, single-input-single-output (SISO) and multiple-input-multiple-output (MIMO) models are built. Simulation results indicate a 3-5 dB improvement in channel estimation accuracy. The suboptimal MMSE equalization results are close to the optimal MMSE with about four orders of magnitude reduction in complexity.

1. Introduction

Future wireless systems must support a wide range of communication requirements, including enhanced Mobile Broadband (eMBB) communication and Ultra-Reliable Low Latency communications (URLLC) [1–3] etc. The Offset Quadrature Amplitude Modulation-based Filter Bank Multi-carrier (OQAM-FBMC) technique enables a flexible selection for prototype filters with acceptable time–frequency properties to minimize spectral sidelobes. Also, prototype filters can be designed to adjust the signal waveform to meet various transmission requirements. OQAM-FBMC system requires no Cyclic Prefixe (CP) and has low bandwidth efficiency minimization for short packet data transfer, making it suitable for 5G applications [4]. Many scholars consider the OQAM-FBMC technology as a candidate for 5G, and OQAM-FBMC is included as a research priority in EU projects such as 5GNOW, PHYDYAS [5–7], etc. Though the Third Generation Partnership Project (3GPP) does not adopt OQAM-FBMC as the new waveform for 5G New Radio (NR), this technique is still an important choice for the development of future wireless systems, such as Carrier Aggregation, Cognitive Radio, and Dense Wavelength Division Multiplexing-based Passive Optical Networks (DWDM-PON) [8–10], etc.

However, the OQAM-FBMC system faces challenging channel estimation and equalization over a doubly selective channel. Due to the high mobility and abundant scatterers, the wireless channels suffer from time-selective fading and frequency-selective fading, called “doubly selective channel” [11,12]. The doubly selective channel response usually varies significantly over a single symbol duration, and there are many channel coefficients. This has become a topical issue for scholars to research [13–18]. The orthogonality of OQAM-FBMC holds only in real domain. Thus, many channel estimation schemes for Orthogonal Frequency Division Multiplexing (OFDM) cannot be used directly. On the other hand, the inherent imaginary interference leads to a complex design for the pilot symbols, which causes the problem of increased difficulty in channel estimation for the OQAM-FBMC

* Corresponding author at: College of Information and Communication Engineering, Harbin Engineering University, Harbin 150001, China.
E-mail addresses: Darius0412@163.com (Y. Wang), guoqiang@hrbeu.edu.cn (Q. Guo), xiangjianhong@hrbeu.edu.cn (J. Xiang).

https://doi.org/10.1016/j.phycom.2023.102120
1874-4907/

system. To simplify the pilot pattern design and improve the channel estimation accuracy, Eleftherios Kofidis et al. [19] proposed a preamble-based channel estimation scheme, where the Interference Approximation Method (IAM) is widely used as a classical method. However, the inherent interference induced by the data symbols to the pilot symbols is unknown, leading to a degradation of the IAM performance and thus the channel estimation performance. Da Chen et al. [20] presented a channel estimation method without guarded symbols and given an optimized structure-pairwise pilot. The method simplifies estimation complexity. However, pairwise pilots can only handle the case in which two-time slots have approximately equal channel information. In fast-time variant channels, the channel information for the two-time slots is different. The pairwise pilot cannot accurately react to the channel information, leading to reduced accuracy for channel estimation. Many scholars have investigated the inherent interference of the pilot symbols and presented channel estimation schemes for auxiliary symbols [21,22]. Unfortunately, it requires sacrificing some time–frequency blocks to transmit auxiliary symbols, reducing bandwidth efficiency. Moreover, the conclusion of [23] indicates that the auxiliary symbol scheme has an undesirable Bit Error Rate (BER), i.e., the channel estimation accuracy is low. A compressed sensing-based channel estimation scheme is presented in [24], which considers the sparsity of the channel, but still begins with the auxiliary symbol method. The auxiliary symbol method requires sacrificing 18–21 time–frequency blocks to construct the Inter-carrier Interference (ICI)-free structure over a doubly selective channel. Therefore, this scheme suffers from low spectral efficiency and inaccurate channel estimation. Defeng Ren et al. [25] proposed a joint channel estimation and equalization method based on a new Analysis Filter Bank (AFB) output signal model, which can use the data symbols reconstructed in real-time as the pilots. However, the method is validated only in frequency-selective fading channels without considering time-selective fading. On the other hand, the Normalized Mean Square Error (NMSE) of the method only reaches -30 dB over a high frequency selective fading channel, which is not a satisfactory result. Prem Singh et al. [26] proposed a doubly selective channel estimation method based on sparse Bayesian learning, which can be applied to Multiple-input Multiple-output (MIMO). However, this method has a high complexity and, over a doubly selective channel, the NMSE can only reach -25 dB.

Over a doubly selective channel, interference is not negligible, i.e., it dominates compared to noise. Therefore, the OQAM-FBMC system equalization must mitigate the impact of ISI, thus ensuring the performance of the whole system. The parallel Fast Fourier Transform (FFT) block equalization method presented in [27] requires constructing multiple parallel FFT modules. At the same time, the equalization technique in [28] requires a larger FFT. Therefore, the technique suffers from high complexity. Simple Zero-forcing (ZF) equalization is easy to implement, but its performance is not good at high noise and interference power. Due to the pure imaginary interference in the OQAM-FBMC system, the complex MMSE cannot be used directly. Therefore, Dirk S. Waldhauser et al. [29] suggested putting the real and imaginary parts in a large matrix for block equalization. Ronald Nissel et al. [30] further improved and presented multi-tap MMSE equalization and full-block MMSE equalization. The multi-tap equalization scheme can mitigate interference from adjacent time symbols and adjacent subcarriers. However, multi-tap equalization mitigation schemes have no fixed criteria. Full-block equalizer is highly complex in large data volumes and multiple subcarriers. Davide Mattera et al. [31] derived the optimal single-tap gain in the MMSE sense, which can obtain better performance than the existing single-tap equalization schemes. However, by considering the impact of Inter-symbol Interference (ISI), the scheme can further improve the BER performance. A sliding window equalization scheme was proposed in [32]. In multipath transmission, the scheme achieves the low-complexity requirement for equalization. However, channel-induced interference needs to be mitigated to improve BER performance when transmitting over a doubly selective channel.

To address the above issues, this paper focuses on channel estimation and equalization schemes for ICI/ISI mitigation. The main contributions are summarized as follows:

- This paper constructs a 2-D channel model for OQAM-FBMC. Firstly, we fit the channel and design the pilot structure. ICI mitigation is achieved by adding guard pilots. Secondly, we optimize the pilot indexes to make the measurement matrix satisfy the better Mutual Coherence Property (MCP). Finally, we utilize the presented Sparse Adaptive Orthogonal Subspace Pursuit (SAOSP) algorithm to recover sparse coefficients, thus obtaining higher accuracy channel estimation. See Section 3.
- This paper presents a threshold judgment suboptimal MMSE equalization scheme. Firstly, we mitigate ISI by estimating the ISI dimension based on the normalized interference power threshold. Secondly, the equalization dimension is flexibly adjusted according to the estimated value, thus reducing the equalization data. Finally, we integrate the equalization data and reduce the matrix dimension, thus reducing the inverse time complexity. See Section 4.
- This paper presents a verification method for applying the OQAM-FBMC system practically. We develop a channel estimation and equalization implementation method for the OQAM-FBMC system employing the new 3GPP 38.900 channel model as the practical channel information. For the simulation verification, we adopt the power delay profile of the "Vehicular A" channel model, and the BER performance is up to 10^{-3} for both Single-input Single-output (SISO) and MIMO. See Section 5.

Notations: Bold capital letters and lowercase letters denote matrices and vectors, respectively. diag$\{\cdot\}$ denotes the diagonal elements of a matrix or generates a diagonal matrix. $\otimes$ represents the Kronecker product. The superscripts $(\cdot)^{-1}$, $(\cdot)^{\dagger}$, $(\cdot)^{*}$, $(\cdot)^{T}$ and $(\cdot)^{H}$ denote inverse, pseudo-inverse, conjugate, transposition and conjugate transposition operators, respectively. E$\{\cdot\}$ indicates expectation. $\Re\{\cdot\}$ and $\Im\{\cdot\}$ denote the real and imaginary parts of the complex variables, respectively. $[\mathbf{c}]_i$ denotes its i-th element. $\mathbf{c}_{1:j}$ denotes its 1st to i-th elements. $\mathbf{I}_L \in \mathbb{C}^{L\times L}$ denotes identity matrix. $[\mathbf{A}]_{i,j}$, $[\mathbf{A}]_i$ and $[\mathbf{A}]_{:,j}$ denote its (i,j) entry, i-th row and j-th column, respectively. The imaginary unit is denoted by $\mathrm{j} = \sqrt{-1}$. The complex domain is denoted as $\mathbb{C}$, and $\mathbb{R}$ denotes the real domain.

2. System model

The OQAM-FBMC system can only transmit real-valued symbols [33]. If the transmitted signal $s(t)$ consists of L subcarriers and K symbols, it can be expressed as

$$s(t) = \sum_{l=1}^{L}\sum_{k=1}^{K} x_{l,k} \underbrace{p_{TX}(t-kT)\mathrm{e}^{\mathrm{j}2\pi lF(t-kT)}\mathrm{e}^{\mathrm{j}\frac{\pi}{2}(l+k)}}_{g_{l,k}(t)}. \tag{1}$$

Where l denotes the frequency position and k the time position. $x_{l,k}$ denotes the transmitted symbol. $p_{TX}(t)$ denotes the transmitted prototype filter function. T represents the time spacing and F the frequency spacing. $\mathrm{e}^{\mathrm{j}2\pi lF(t-kT)}$ denotes the frequency shift

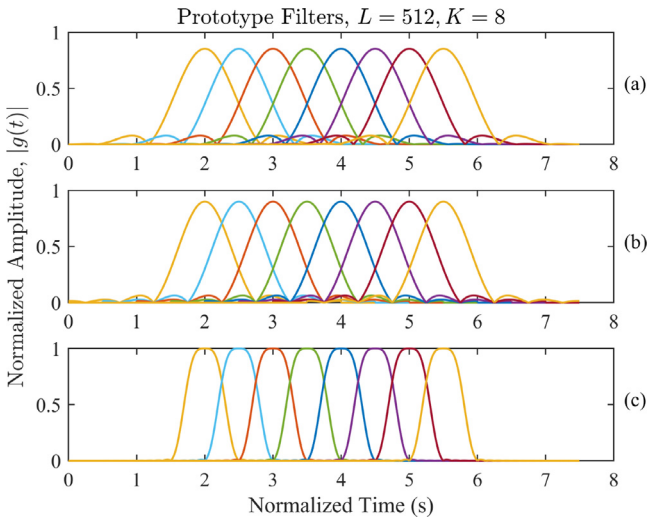

Fig. 1. Time domain waveforms of different prototype filters. (a) PHYDYAS prototype filter, (b) IOTA prototype filter, (d) Sinc function-based prototype filter.

factor and $e^{j\frac{\pi}{2}(l+k)}$ the phase shift factor. $g_{l,k}(t)$ denotes the transmitted base pulses. An available prototype filter for OQAM-FBMC is based on the Sinc function, expressed as

$$p(t) = \sqrt{\frac{2}{T_0}} \sum_{i=-O+1}^{O-1} \varphi_i \text{sinc}(\frac{2O}{T_0}\text{sign}(i)t + \frac{kT_0}{2O}) . \tag{2}$$

Where O indicates the overlapping factor. T_0 represents a time-scaling parameter, which depends on the time spacing. sign(i) denotes a symbolic function. Note that, in this paper, we take sign(0) = 1. The calculation of the coefficients φ depends on the overlapping factor O. For example, when $O = 5$, the coefficients are

$$\begin{cases} \varphi_0 = 1 \\ \varphi_1 = \varphi_{-1} = 0.99184131 \\ \varphi_2 = \varphi_{-2} = 0.86541624 \\ \varphi_3 = \varphi_{-3} = 0.50105361 \\ \varphi_4 = \varphi_{-4} = 0.12747868 . \end{cases} \tag{3}$$

Compared to the IOTA prototype filter [34] and the PHYDYAS prototype filter [35], this paper uses the prototype filter with small time domain ripple, see Fig. 1, and less interference symbols to be considered for equalization.

In OQAM-FBMC, the received prototype filter function $p_{RX}(t) = p_{TX}(t)$. At time $t \in [-OT_0/2, OT_0/2 + (K-1)T)$, we sample the base pulse with the rate $f_s = 1/\Delta t$. The discrete-time expression for the transmitted signal is

$$s(n) = \sqrt{\Delta t} \sum_{k=1}^{K} \sum_{l=1}^{L} x_{l,k} g_{l,k}((n-1)\Delta t - \frac{OT_0}{2}). \tag{4}$$

Where $n = 1, \ldots, N$. $N = (OT_0 + T(K-1))f_s$ denotes the total number of samples and Δt the sampling time spacing. For a doubly selective channel, we assume that the channel contains U propagation paths and the Doppler shifts and delays of each path $u = 1, \ldots, U$ are ν_u and τ_u, respectively. Then, the discrete time-variant impulse response of the channel is given by [36], expressed as

$$h(n, m) = \sum_{u=1}^{U} \eta_u e^{j2\pi\nu_u n\Delta t} \text{sinc}(\pi(m - \tau_u f_s)). \tag{5}$$

Where η_u denotes the path attenuation and initial phase of the u-th path, and $m = 1, \ldots, M$ the channel tap. As the discrete transmitted signal $s(n)$ passes through the channel, the discrete received signal $r(n)$ is obtained, expressed as

$$r(n) = \sum_{m=1}^{M} h(n-m, m)s(n) + w(n). \tag{6}$$

Where $w(n) \sim \mathcal{CN}(0, P_n)$ denotes the discretized noise and P_n the noise power in time. Projecting $r(n)$ to the discrete received base pulse, we can obtain the received data symbol $y_{l,k}$, expressed as

$$y_{l,k} = \sqrt{\Delta t} \sum_{n=1}^{N} r(n) g^*_{l,k}((n-1)\Delta t - \frac{OT_0}{2}). \tag{7}$$

To describe the system more conveniently, we denote the base pulse samples by a vector $\mathbf{g}_{l,k} \in \mathbb{C}^{N\times 1}$ and integrate the sample vectors into a transmission matrix $\mathbf{G} = [\mathbf{g}_{1,1}, \ldots, \mathbf{g}_{L,K}] \in \mathbb{C}^{N\times LK}$. Similarly, $\mathbf{x} = [x_{1,1}, \ldots, x_{L,K}]^T \in \mathbb{R}^{LK\times 1}$ denotes the transmitted data symbol vector, and then the received data symbol vector $\mathbf{y} = [y_{1,1}, \ldots, y_{L,K}]^T \in \mathbb{C}^{LK\times 1}$ can be expressed as

$$\mathbf{y} = \mathbf{G}^H\mathbf{H}\mathbf{G}\mathbf{x} + \mathbf{W}. \tag{8}$$

Where $\mathbf{H} \in \mathbb{C}^{N\times N}$ denotes the time-variant convolution matrix and $\mathbf{W} \sim \mathcal{CN}(0, P_n\mathbf{G}^H\mathbf{G})$ the Gaussian noise. The orthogonality of OQAM-FBMC holds only in the real domain, i.e., $\Re\{\mathbf{G}^H\mathbf{G}\} = \mathbf{I}_{LK}$. Thus, $\mathbf{G}^H\mathbf{H}\mathbf{G} \in \mathbb{C}^{LK\times LK}$ is pseudo-cyclic and is a full matrix instead of a diagonal matrix in the transformation domain. This leads to ICI/ISI. On the other hand, assuming a 2 × 2 MIMO system, we can model it as

$$\begin{bmatrix} \mathbf{y}_1 \\ \mathbf{y}_2 \end{bmatrix} = \begin{bmatrix} \mathbf{G}^H\mathbf{H}^{1,1}\mathbf{G} & \mathbf{G}^H\mathbf{H}^{1,2}\mathbf{G} \\ \mathbf{G}^H\mathbf{H}^{2,1}\mathbf{G} & \mathbf{G}^H\mathbf{H}^{2,2}\mathbf{G} \end{bmatrix} \begin{bmatrix} \mathbf{x}_1 \\ \mathbf{x}_2 \end{bmatrix} + \begin{bmatrix} \mathbf{W}_1 \\ \mathbf{W}_2 \end{bmatrix}. \tag{9}$$

Where $\mathbf{H}^{i,j}$ denotes the time-variant convolution matrix from the transmitted antenna i to the received antenna j.

3. Channel estimation

The channel estimation performance is reduced when the pilot subcarrier suffers from interference. Therefore, we need to investigate ICI mitigation schemes to solve the interference issue and then, improve the channel estimation performance.

3.1. 2-D channel modeling

Assuming that the total channel taps are M, we define $\mathbf{h}_m \triangleq [h(1, m), \ldots, h(L, m)]^T$ to represent the time-variant property of the m-th channel tap. Then, $\mathbf{h}_m$ can be expressed as [37]

$$\mathbf{h}_m = \underbrace{\begin{bmatrix} \mathbf{b}_1 & \mathbf{b}_2 & \cdots & \mathbf{b}_Q \end{bmatrix}}_{\mathbf{B}} \begin{bmatrix} c_{1,m} \\ c_{2,m} \\ \vdots \\ c_{Q,m} \end{bmatrix} + \boldsymbol{\zeta}_m. \tag{10}$$

Where $\mathbf{B} \in \mathbb{C}^{L\times Q}$ denotes a basis function matrix and $c_{q,m}$ the Basis Expansion Model (BEM) coefficient. $\boldsymbol{\zeta}_m \triangleq [\zeta(1, m), \ldots, \zeta(L, m)]^T$ denotes channel fitting error. We consider the case of L subcarriers and define $\mathbf{h}'_l \triangleq [h(l, 1), \ldots, h(l, M)]^T$ to denote the time-variant channel corresponding to the l-th subcarrier. $\mathbf{c}_q = [c_{q,1}, \ldots, c_{q,M}]^T \in \mathbb{C}^{M\times 1}$ denotes the q-th order BEM coefficient vector and $\boldsymbol{\zeta}'_l \triangleq [\zeta(l, 1), \ldots, \zeta(l, M)]^T$. Then, the matrix form of Eq. (10) can be expressed as

$$\tilde{\mathbf{H}} = (\mathbf{B} \otimes \mathbf{I}_M)\mathbf{C} + \boldsymbol{\zeta}. \tag{11}$$

Where $\tilde{\mathbf{H}} \triangleq [\mathbf{h}_1'^T, \ldots, \mathbf{h}_L'^T]^T \in \mathbb{C}^{LM\times 1}$, $\mathbf{C} \triangleq [\mathbf{c}_1^T, \ldots, \mathbf{c}_Q^T]^T \in \mathbb{C}^{QM\times 1}$, $\boldsymbol{\zeta} \triangleq [\boldsymbol{\zeta}_1'^T, \ldots, \boldsymbol{\zeta}_L'^T]^T$. Basis function matrix $\mathbf{B} \in \mathbb{C}^{L\times Q}$ is expressed as

$$\mathbf{B} = \begin{bmatrix} 1 & \cdots & e^{j\frac{2\pi}{L}(L-1)(1-\frac{Q}{2})} \\ \vdots & \ddots & \vdots \\ 1 & \cdots & e^{j\frac{2\pi}{L}(L-1)(Q-\frac{Q}{2})} \end{bmatrix}^T . \tag{12}$$

According to the Distributed Compressive Sensing (DCS) theory [38], it is known that the channel is sparse in the transform domain. Therefore, we assume that the q-th order basis function matrix $\mathbf{B}_q \in \mathbb{C}^{L\times L}$ and the diagonal matrix $\mathbf{C}_q \in \mathbb{C}^{L\times L}$ of channel coefficients are

$$\mathbf{B}_q = \mathbf{F}_L \mathrm{diag}\{\mathbf{b}_q\}\mathbf{F}_L^H, \tag{13}$$

$$\mathbf{C}_q = \mathrm{diag}\{\sqrt{L}\mathbf{F}_L(\mathbf{c}_q^T, \mathbf{0}_{1\times(L-M)})^T\}. \tag{14}$$

Where $\mathbf{F}_L$ denotes the L-order discrete Fourier transform matrix. However, if we want to explore the channel sparsity and complete the 2-D channel modeling of the OQAM-FBMC system, we also require an inverse Fourier transform for the transmitted signal. This scheme is feasible because it can reduce the peak-to-average power ratio [39]. Therefore, for a full matrix in the transform domain, if only $K = 1$ time symbol is transmitted, then Eq. (8) can be expressed as [38]

$$\begin{aligned} \mathbf{y} &= \mathbf{G}^H\mathbf{H}\mathbf{G}\mathbf{x} + \mathbf{W} \\ &= \left(\sum_{q=1}^{Q} \mathbf{B}_q\mathbf{C}_q\right)\mathbf{F}_L^H\mathbf{x} + \mathbf{W}. \end{aligned} \tag{15}$$

Note that the OQAM-FBMC system transmission is continuous and has strong symbol overlap, however, the modeling of Eq. (15) fails to mitigate the ISI. Therefore, we need to explore ISI mitigation schemes, see Section 5. On the other hand, we do not consider that the assignment of the pilot is two-dimensional (time–frequency frame). We consider placing guard pilots about effective pilots, thus mitigating ICI. Therefore, it is necessary to build the pilot structure and optimize the pilot index.

3.2. Pilot structure and index optimization

The total number of pilot subcarriers and the corresponding indexes are denoted by P and ϑ, respectively. The index set of the effective pilot subcarrier vector $\mathbf{P}_{\mathrm{ef}} \in \mathbb{C}^{\mathcal{I}}$ is $\vartheta_{\mathrm{ef}} = [\vartheta_1, \ldots, \vartheta_{\mathcal{I}}]$. Its cardinality is $|\vartheta_{\mathrm{ef}}| = \mathcal{I}$ (Note that $S < \mathcal{I} \ll M$, S denotes sparsity). The index set of the guard pilot subcarrier vector $\mathbf{P}_{\mathrm{guard}} \in \mathbb{C}^{(2Q-2)\mathcal{I}}$ is $\vartheta_{\mathrm{guard}}$. Its cardinality is $|\vartheta_{\mathrm{guard}}| = (2Q-2)\mathcal{I}$. Therefore, $P = |\vartheta_{\mathrm{ef}}| + |\vartheta_{\mathrm{guard}}| = (2Q-1)\mathcal{I}$, and $\vartheta_{\mathrm{ef}} \cup \vartheta_{\mathrm{guard}} = \vartheta$. Assigning all the pilot indices to Q subsets, we can obtain

$$\begin{cases} \vartheta_1 = \vartheta_{\mathrm{ef}} - (Q+1)/2 \\ \quad\vdots \\ \vartheta_{(Q+1)/2} = \vartheta_{\mathrm{ef}} \\ \quad\vdots \\ \vartheta_Q = \vartheta_{\mathrm{ef}} + (Q+1)/2\ . \end{cases} \tag{16}$$

Note that when $i \neq j$, $|\vartheta_i - \vartheta_j| \geq 2Q-1$. Utilizing the above pilot structure, we can decouple the BEM coefficients $\mathbf{c}_q \big|_{q=1}^{Q}$ by Eq. (15), and the ICI is mitigated.

$$\underbrace{\begin{bmatrix}[\mathbf{R}]_{\vartheta_1} \\ \vdots \\ [\mathbf{R}]_{\vartheta_Q}\end{bmatrix}}_{\mathbf{Y}} = \underbrace{\tilde{\mathbf{P}}_{\mathrm{ef}} \otimes \begin{bmatrix}[\mathbf{F}_L']_{\vartheta_1} & \cdots & 0 \\ \vdots & \ddots & \vdots \\ 0 & \cdots & [\mathbf{F}_L']_{\vartheta_Q}\end{bmatrix}}_{\boldsymbol{\Phi}'} \begin{bmatrix}\mathbf{c}_1 \\ \vdots \\ \mathbf{c}_Q\end{bmatrix} + \underbrace{\begin{bmatrix}\mathbf{W}_1 \\ \vdots \\ \mathbf{W}_2\end{bmatrix}}_{\boldsymbol{\eta}} . \tag{17}$$

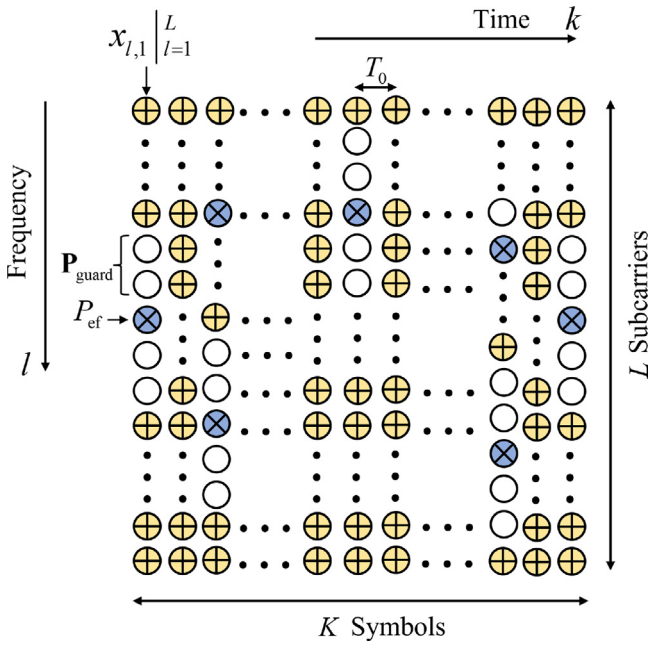

Fig. 2. OQAM-FBMC frame structure in SISO systems. The notations ⊗, ◯ and ⊕ indicate effective pilots, guard pilots and data, respectively.

Where $[\mathbf{R}]_{\vartheta_q}$ denotes the subset of the received OQAM-FBMC subcarriers $\mathbf{R}$, $\tilde{\mathbf{P}}_{\mathrm{ef}} \triangleq \mathrm{diag}\{\mathbf{P}_{\mathrm{ef}}\}$. The submatrix $[\mathbf{F}_L']_{\vartheta_q} = [\sqrt{L}\mathbf{F}_L]_{\vartheta_q,1:M}$, and $\mathbf{W}_q \big|_{q=1}^{Q}$ contains noise and modeling errors. From the structure of Eq. (17), it is possible to estimate the channel coefficients using DCS theory. However, there is still a problem in that BEM coefficients of different orders correspond to different measurement matrices. To address this issue, we further investigate the relationship between the effective and the guard pilot index submatrix of FFT. The truncated FFT submatrix $\mathbf{F}_L' \in \mathbb{C}^{L\times M}$ can be expressed as

$$\mathbf{F}_L' = \begin{bmatrix} 1 & 1 & \cdots & 1 \\ 1 & \varpi & \cdots & \varpi^{M-1} \\ \vdots & \vdots & \ddots & \vdots \\ 1 & \varpi^{L-1} & \cdots & \varpi^{(L-1)(M-1)} \end{bmatrix} . \tag{18}$$

Where $\varpi \triangleq e^{j2\pi/L}$. The FFT submatrix of the q-th pilot index $[\mathbf{F}_L']_{\vartheta_q}$ can be written as

$$\begin{aligned} [\mathbf{F}_L']_{\vartheta_q} &= [\mathbf{F}_L']_{\vartheta_{\frac{Q+1}{2}}} \begin{bmatrix} 1 & 0 & \cdots & 0 \\ 0 & \varpi^{q-\frac{Q+1}{2}} & \cdots & 0 \\ \vdots & \vdots & \ddots & \vdots \\ 0 & 0 & \cdots & \varpi^{(q-\frac{Q+1}{2})(M-1)} \end{bmatrix} \\ &= [\mathbf{F}_L']_{\vartheta_{\frac{Q+1}{2}}} \boldsymbol{\Lambda}_q\ . \end{aligned} \tag{19}$$

Note that when $q = (Q+1)/2$, $\boldsymbol{\Lambda}_q = \mathbf{I}_M$. According to Eq. (19), we can rewrite Eq. (17) as

$$\underbrace{\begin{bmatrix}[\mathbf{R}]_{\vartheta_1} \\ \vdots \\ [\mathbf{R}]_{\vartheta_Q}\end{bmatrix}}_{\mathbf{Y}} = \underbrace{[\tilde{\mathbf{P}}_{\mathrm{ef}}[\mathbf{F}_L']_{\vartheta_{\frac{Q+1}{2}}}]}_{\boldsymbol{\Phi}} \otimes \mathbf{I}_Q] \begin{bmatrix}\boldsymbol{\Lambda}_1\mathbf{c}_1 \\ \vdots \\ \boldsymbol{\Lambda}_Q\mathbf{c}_Q\end{bmatrix} + \underbrace{\begin{bmatrix}\mathbf{W}_1 \\ \vdots \\ \mathbf{W}_Q\end{bmatrix}}_{\boldsymbol{\eta}} . \tag{20}$$

Therefore, in the SISO system, the described OQAM-FBMC frame structure is shown in Fig. 2.

According to DCS theory, if $\boldsymbol{\Phi} = \tilde{\mathbf{P}}_{\text{ef}}[\mathbf{F}_L']_{\vartheta_{(Q+1)/2}}$ satisfies the MCP condition [40], we can obtain $\mathbf{c}_q\big|_{q=1}^{Q}$ by estimating $\boldsymbol{\Lambda}_q\mathbf{c}_q\big|_{q=1}^{Q}$. However, the above pilot structure design is completely dependent on the pilot index. Therefore, we present the index stochastic optimization technique, see **Algorithm 1**. This technique enables us to obtain the smallest possible $\mu(\boldsymbol{\Phi})$-value and thus recover the channel coefficients with higher probability. The optimization problem described can be formulated as

$$\begin{aligned} \min_{\vartheta_{\frac{Q+1}{2}}} \quad & \mu(\tilde{\mathbf{P}}_{\text{ef}}[\mathrm{F}_L']_{\vartheta_{\frac{Q+1}{2}}}) \\ st. \quad & |\vartheta_i - \vartheta_j| \geq 2Q-1, \forall i,j, i \neq j\ . \end{aligned} \tag{21}$$

To overcome the coupling of the optimization objective, we use the Constant Amplitude Zero Auto Correlation (CAZAC) sequence as the effective pilot element. This enables the effective pilot to have zero autocorrelation.

Algorithm 1: Pilot index Stochastic Optimization Technique.

Step 1: Randomly generate an effective pilot index $\vartheta_{(Q+1)/2}^{(0)}$ satisfying $|\vartheta_i - \vartheta_j| \geq 2Q-1$.
Step 2: Initialization. $\hat{\vartheta}_{(Q+1)/2}^{(0)} \leftarrow \vartheta_{(Q+1)/2}^{(0)}$, $\alpha \leftarrow 0$ and $\beta \leftarrow 0$, $[\boldsymbol{\lambda}]_0 \leftarrow \mathbf{0}$, $[\boldsymbol{\lambda}]_{0,0} \leftarrow 1$.
Step 3: Iteration.
for $t = 1, \cdots, A\mathcal{I}$ **do**
  a) Generate another effective pilot index.
  $\tilde{\vartheta}_{(Q+1)/2}^{(t)} \leftarrow rand.\ \ st.\ \tilde{\vartheta}_{(Q+1)/2}^{(t)} \neq 0$,
  $\min(\tilde{\vartheta}_{(Q+1)/2}^{(t)} - \vartheta_{\text{ef}}) \geq 5,\ |\vartheta_i - \vartheta_j| \geq 2Q-1$.
  b) Optimization.
  if $\mu(\tilde{\mathbf{P}}_{\text{ef}}[\mathbf{F}_L']_{\tilde{\vartheta}_{(Q+1)/2}^{(t)}}) < \mu(\tilde{\mathbf{P}}_{\text{ef}}[\mathbf{F}_L']_{\vartheta_{(Q+1)/2}^{(t)}})$ **then**
    $\vartheta_{(Q+1)/2}^{(t+1)} \leftarrow \tilde{\vartheta}_{(Q+1)/2}^{(t)},\ \alpha \leftarrow t+1$.
  else
    $\vartheta_{(Q+1)/2}^{(t+1)} \leftarrow \vartheta_{(Q+1)/2}^{(t)}$.
  end
  c) Status Update. $[\boldsymbol{\lambda}]_{t+1} = [\boldsymbol{\lambda}]_t + [\delta]_{t+1}([\Delta]_{t+1} - [\boldsymbol{\lambda}]_t)$, The reduction step is $[\delta]_t = 1/t$.
  d) Select the optimal pilot index.
  if $[\boldsymbol{\lambda}]_{t+1,\alpha} > [\boldsymbol{\lambda}]_{t+1,\beta}$ **then**
    $\hat{\vartheta}_{(Q+1)/2}^{(t+1)} \leftarrow \vartheta_{(Q+1)/2}^{(t+1)}, \beta \leftarrow \alpha$.
  else
    $\hat{\vartheta}_{(Q+1)/2}^{(t+1)} \leftarrow \hat{\vartheta}_{(Q+1)/2}^{(t)}$.
  end
end
return Effective Pilot index $\vartheta_{\text{ef}} = [\hat{\vartheta}_1, \cdots, \hat{\vartheta}_{\mathcal{I}}]$.

In **Algorithm 1**, $\vartheta_{(Q+1)/2}^{(t)}$, $\hat{\vartheta}_{(Q+1)/2}^{(t)}$, $\hat{\vartheta}_{(Q+1)/2}^{(t)}$ are defined as the pilot indexes of the t-th iteration. $A\times\mathcal{I}$ is the number of iterations, and A is an empirical value. $[\Delta]_t$ is defined as a zero vector, but its t-th element is 1. The column elements of the probability matrix $\boldsymbol{\lambda}$ have property $\sum_j \lambda_{i,j} = 1$. The restriction $\min(\tilde{\vartheta}_{(Q+1)/2}^{(t)} - \vartheta_{\text{ef}}) \geq 5$ ensures that the effective pilot index does not overlap with the guard pilot index. The complexity of **Algorithm 1** is quite low because it does not require inverse operations and only numerical comparisons are needed.

From the above analysis, the channel coefficient estimation problem can be solved by DCS theory. A subspace pursuit (SP) [41] algorithm can be applied to our framework. However, the size of its subspace depends on the sparsity. Based on SP, we present the sparse adaptive orthogonal subspace pursuit (SAOSP) algorithm. Its steps are indicated by **Algorithm 2**.

Algorithm 2: The SAOSP based Coefficients Estimation.

Input: $\mathbf{Y}_q = [\mathbf{R}]_{\vartheta_q}\big|_{q=1}^{Q}$, Measurement Matrix
$\boldsymbol{\Phi} = \tilde{\mathbf{P}}_{\text{ef}}[\mathbf{F}_L']_{\vartheta_{(Q+1)/2}}$.
Output: $\hat{\mathbf{c}}_q\big|_{q=1}^{Q}$.

1 **Step 1:** Initialize index set $\Omega^{(0)} = 0$, Choose columns of the matrix $\mathbf{B}^{(0)} = \varnothing$, The residual $\mathbf{r}^{(0)} = \mathbf{Y}_q$, Iteration Count $t = 1$, and recovery error $err = 10^{-5}$.
2 **Step 2:** Determine the subspace dimension D.
$c_{low} \leftarrow \frac{2}{M}\sum_{m=1}^{M}[|\boldsymbol{\Phi}^T\mathbf{Y}_q|]_m$, $D \leftarrow size(|\boldsymbol{\Phi}^T\mathbf{Y}_q| \geq c_{low})$.
3 **Step 3:** Subspace orthogonal projection.
$[\mathbf{c}_{or}]^{(t)} \leftarrow \boldsymbol{\Phi}^T\mathbf{r}^{(t)}$, Arrange $|[\mathbf{c}_{or}]^{(t)}|$ in ascending order and get the position index $\vartheta^{(t)}$. $\Omega^{(t)} \leftarrow \vartheta_{1:D}^{(t)}$, $\mathbf{B}^{(t)} \leftarrow \boldsymbol{\Phi}_{\Omega^{(t)}}$, $\mathbf{x}^{(t)} \leftarrow \left(\mathbf{B}^{(t)}\right)^{\dagger}\mathbf{Y}_q$.
4 **Step 4:** Status update.
Arrange $|\mathbf{x}^{(t)}|$ in ascending order and update the position index to $\vartheta^{(t+1)}$. $\Omega^{(t+1)} \leftarrow \vartheta_{1:D}^{(t+1)}$, $\mathbf{B}^{(t+1)} \leftarrow \boldsymbol{\Phi}_{\Omega^{(t+1)}}$.
Calculate the residual $\mathbf{r}^{(t+1)} = \mathbf{Y}_q - \left(\mathbf{B}^{(t+1)}\right)^{\dagger}\mathbf{Y}_q$.
5 **Step 5:** Repeat Step3- Step4 until $\mathbf{r}^{(t)} \leq err$.
6 **Step 6:** Obtain $\hat{\mathbf{c}}_q\big|_{q=1}^{Q}$ from $\hat{\boldsymbol{\Lambda}}_q\hat{\mathbf{c}}_q\big|_{q=1}^{Q}$ using Least Square (LS) method.

The Algorithm needs to run Q times to recover all BEM coefficients. This algorithm has a certain complexity because it requires inverse operations. Considering the inverse time complexity, the complexity of **Algorithm 2** to estimate all coefficients can be expressed as $\mathcal{O}(2Q^3D^3)$ (note that two pseudo-inversions are required for each iteration). Usually, the complexity of the SAOSP algorithm is the same as the SP algorithm because the channel sparsity is the same. On the other hand, the feasibility of DCS theory implies that Compressive Sensing (CS) theory is also applicable. Therefore, popular algorithms such as Orthogonal Matching Pursuit (OMP) are also applicable. However, the presented algorithm is more advantageous in terms of reconstruction probability, see Section 5.

4. Equalization scheme

The OQAM-FBMC system transmission is continuous and there is significant symbol overlap. To approach the optimal probability of symbol detection, we need to mitigate the ISI. When transmitting massive time symbols, we reconsider that the distribution of symbols is two-dimensional. Using the variability of the interference power, we can determine the number of interference symbols. This allows us to design effective equalization schemes.

We denote the considered received symbols by $\mathbf{y}_\zeta \in \mathbb{C}^{|\zeta|\times 1}$, which contains a reference symbol and some interference symbols. Let $\boldsymbol{\mathcal{H}} = \mathbf{G}^H\mathbf{H}\mathbf{G}$, and then split the transmission model of Eq. (8) as

$$\mathbf{y}_\zeta = \boldsymbol{\mathcal{H}}_\zeta\mathbf{x}_\zeta + \boldsymbol{\mathcal{H}}_{\zeta,\mathcal{R}}\mathbf{x}_{\mathcal{R}} + \mathbf{W}_\zeta. \tag{22}$$

Where $\boldsymbol{\mathcal{H}}_\zeta \in \mathbb{C}^{|\zeta|\times|\zeta|}$. $\mathbf{x}_\zeta \in \mathbb{R}^{|\zeta|\times 1}$ denotes the considered transmitted symbols. $\boldsymbol{\mathcal{H}}_{\zeta,\mathcal{R}} \in \mathbb{C}^{|\zeta|\times|\mathcal{R}|}$. $\mathbf{x}_{\mathcal{R}} \in \mathbb{R}^{|\mathcal{R}|\times 1}$ denotes all remained symbols. Usually, $|\zeta| \ll LK$. Considering the existence of noise in the system, we need to calculate the base pulse correlation matrix $\mathbf{R}_{\text{b}} \in \mathbb{C}^{2LK\times 2LK}$, which can be expressed as

$$\mathbf{R}_{\text{b}} = \begin{bmatrix} \Re\{\mathbf{G}^H\mathbf{G}\} & -\Im\{\mathbf{G}^H\mathbf{G}\} \\ \Im\{\mathbf{G}^H\mathbf{G}\} & \Re\{\mathbf{G}^H\mathbf{G}\} \end{bmatrix}. \tag{23}$$

The presented suboptimal MMSE equalizer with threshold judgment is expressed as

$$\hat{\mathbf{x}}_\zeta = \begin{bmatrix} \Re\{\boldsymbol{\mathcal{H}}_\zeta\} \\ \Im\{\boldsymbol{\mathcal{H}}_\zeta\} \end{bmatrix}^T \left(\mathbf{H}_\Delta + \frac{P_n}{2} \mathbf{R}_{\mathrm{b},\zeta} \right)^{-1} \begin{bmatrix} \Re\{\mathbf{y}_\zeta\} \\ \Im\{\mathbf{y}_\zeta\} \end{bmatrix}, \tag{24}$$

$$\mathbf{H}_\Delta = \begin{bmatrix} \Re\{\boldsymbol{\mathcal{H}}_\zeta\} \\ \Im\{\boldsymbol{\mathcal{H}}_\zeta\} \end{bmatrix} \begin{bmatrix} \Re\{\boldsymbol{\mathcal{H}}_\zeta\} \\ \Im\{\boldsymbol{\mathcal{H}}_\zeta\} \end{bmatrix}^T + \begin{bmatrix} \Re\{\boldsymbol{\mathcal{H}}_{\zeta,\mathcal{R}}\} \\ \Im\{\boldsymbol{\mathcal{H}}_{\zeta,\mathcal{R}}\} \end{bmatrix} \begin{bmatrix} \Re\{\boldsymbol{\mathcal{H}}_{\zeta,\mathcal{R}}\} \\ \Im\{\boldsymbol{\mathcal{H}}_{\zeta,\mathcal{R}}\} \end{bmatrix}^T. \tag{25}$$

Where $\mathbf{R}_{\mathrm{b},\zeta} \in \mathbb{C}^{2|\zeta|\times 2|\zeta|}$ denotes the submatrix of $\mathbf{R}_\mathrm{b} \in \mathbb{C}^{2LK\times 2LK}$. Note that $\hat{\mathbf{x}}_\zeta \in \mathbb{R}^{|\zeta|\times 1}$ contains ζ elements. However, we focus only on the reference symbol, while other symbols are dropped as interference. Therefore, the time complexity of the inverse operation can be calculated as $\mathcal{O}(8LK|\zeta|^3)$. The inverse operation time complexity of the optimal MMSE equalization is $\mathcal{O}(8L^3K^3)$.

Using the normalized interference power threshold γ, we can determine the number of transmitted symbols that should be considered. The symbols with normalized interference power higher than the threshold γ all need to be considered. For example, when γ is taken as 10^{-4}, which is sufficient to mitigate most of the symbol interference, the received symbol under consideration can be denoted as $\mathbf{y}_\zeta = [y_{l-2,k-1}, \ldots, y_{l,k}, \ldots y_{l+2,k+1}]^T$. Compared to the optimal MMSE equalizer, the suboptimal MMSE equalizer is much less complex, especially for high subcarrier numbers and large data volumes, and the effect is close to the optimal MMSE. On the other hand, the proposed equalizer can be extended to MIMO systems with desired results.

5. Numerical results

In this section, we numerically analyze the presented channel estimation and equalization approach. For numerical comparison of channel estimation schemes, our comparison algorithms are Orthogonal Matching Pursuit (OMP, 2007) [42], Distributed Compressed Sensing Simultaneous Orthogonal Matching Pursuit (DCS-SOMP, 2013) [38], Regularized Orthogonal Matching Pursuit (ROMP, 2015) [43], Orthogonal Least Squares (OLS, 2016) [44], Multipath Matching Pursuit (MMP, 2020) [45] and Generalized Back tracking Regularized Adaptive Matching Pursuit (GBRAMP, 2021) [46], respectively.

5.1. Reconstruction success rate

We use a 1-D random sparse signal with a length of 1000 and choose a measurement value of 300. The signal reconstruction probability varies with the sparsity S as shown in Fig. 3. When the sparsity S is fixed to 90, the accurate reconstruction probability of the signal varies with the measurement value as shown in Fig. 4.

From Fig. 3, we can see that the presented SAOSP algorithm can accommodate a greater degree of sparsity S. However, near the sparsity $S = 120$, the presented algorithm has a certain disadvantage compared to MMP. This usually has no effect because the channel sparsity is much smaller compared to the length. On the other hand, when the sparsity is fixed, the presented algorithm has a higher reconstruction rate compared to other algorithms, see Fig. 4. Therefore, greater accuracy can be obtained by applying SAOSP to channel coefficients recovery.

5.2. NMSE criteria and BER

To illustrate the case better, we consider a fast-fading channel model (i.e., Vehicular A channel model) and profile the following parameters. The number of channel taps is $M = 50$, the mobile velocity is $V = 200$ km/h, and the number of Wide-sense Stationary Uncorrelated Scattering (WSSUS) is 200. The carrier frequency is 2.5 GHz. The number of transmitted complex

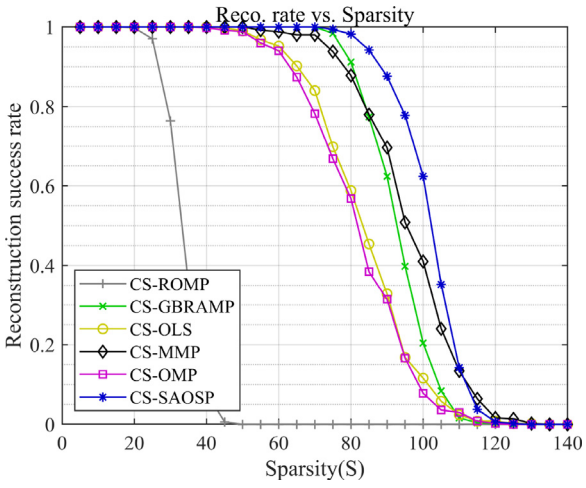

Fig. 3. The signal reconstruction success rate of different algorithms varies with sparsity when the measurement value is 300.

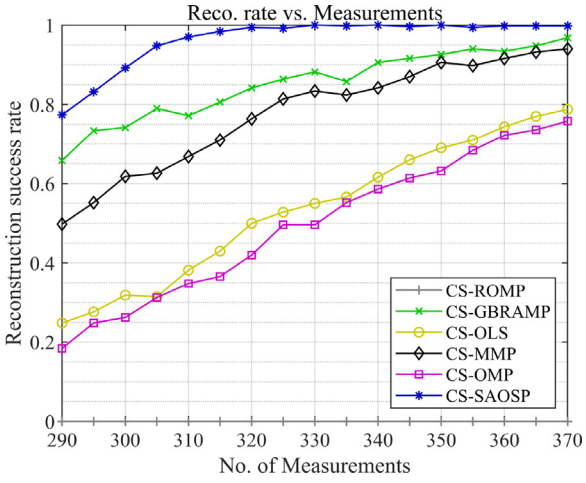

Fig. 4. The signal reconstruction success rate of different algorithms varies with the measurement value when $S = 90$.

symbols is $K = 15$ ($K = 30$ real-valued symbols). The frequency spacing is $F = 15$ kHz, the number of subcarriers is $L = 512$ and assumes that all subcarriers are available for transmission. The number of effective pilots is $\mathcal{I} = 32$, the BEM order is $Q = 3$, and the system modulation is 16-OQAM. The above parameter configuration results in a data transfer time for OQAM-FBMC is $(2K)/(2F) = 1$ ms (note that OQAM-FBMC compresses the time spacing to $T = 0.5/F$).

The expression for NMSE is

$$\mathrm{NMSE}_{\hat{\boldsymbol{\mathcal{H}}}} = \frac{\mathrm{E}\{\|\boldsymbol{\mathcal{H}} - \hat{\boldsymbol{\mathcal{H}}}\|_2^2\}}{\mathrm{E}\{\|\boldsymbol{\mathcal{H}}\|_2^2\}}. \tag{26}$$

Where $\|\cdot\|_2$ denotes the Euclidean norm and $\hat{\boldsymbol{\mathcal{H}}}$ the estimated value. The smaller the NMSE value, the closer the estimated value is to the perfect Channel State Information (CSI). "Perfect-CSI" means that $\boldsymbol{\mathcal{H}}$ is known at the receiver. The NMSE metrics for channel estimation with different algorithms are shown in Fig. 5. DCS-SOMP can simultaneously process Q-order BEM coefficients and thus can achieve better results compared to other CS algorithms. However, the presented SAOSP algorithm has higher

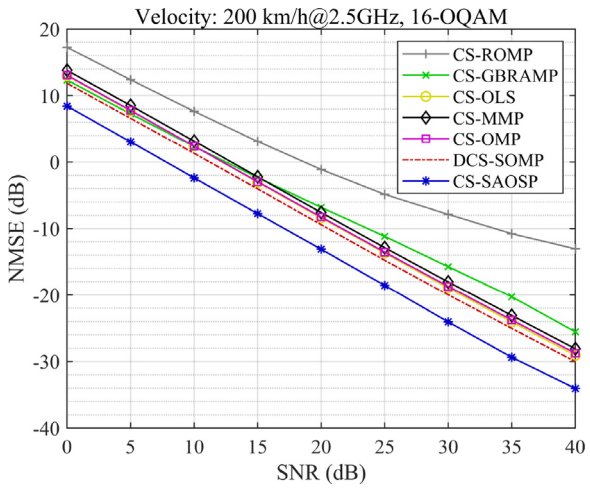

Fig. 5. NMSE metrics for channel estimation with different algorithms. The SAOSP algorithm improves about 3–5 dB in NMSE metrics compared to DCS-SOMP.

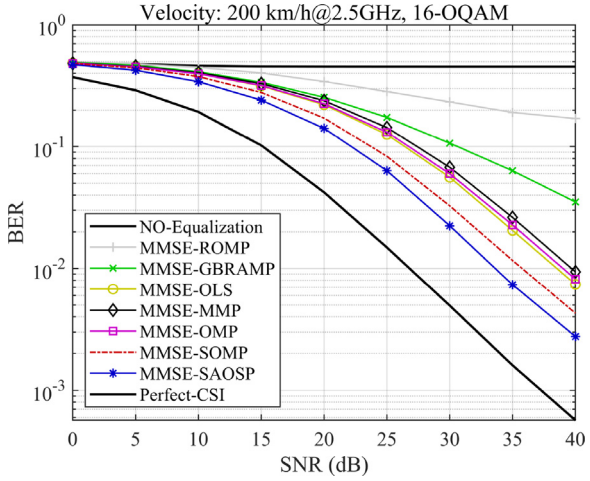

Fig. 6. The BER corresponding to different algorithms under the optimal MMSE equalizer. The presented SAOSP algorithm enables the system to have a lower BER with an improvement of about 0.3%–0.5%.

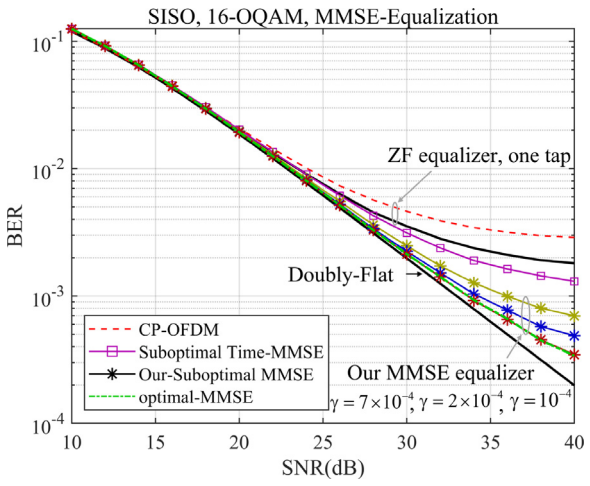

Fig. 7. The BER curves of suboptimal MMSE equalization with different normalized interference power thresholds. The gold curve corresponds to $\gamma = 7 \times 10^{-4}$, the blue curve corresponds to $\gamma = 2 \times 10^{-4}$, and the red curve corresponds to $\gamma = 10^{-4}$.

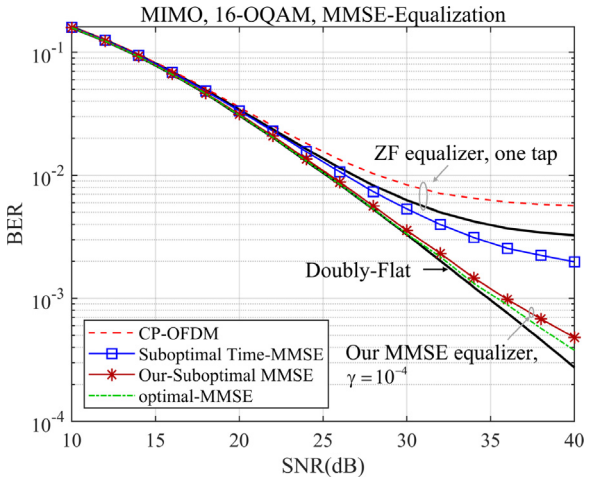

Fig. 8. The BER curves of the suboptimal MMSE equalizer extended to the MIMO system. Only a 2 × 2 MIMO transmission system is considered, and the normalized interference power threshold is considered only for $\gamma = 10^{-4}$.

recovery accuracy as shown in Fig. 5. To approach the optimal symbol detection, we employ the optimal MMSE equalizer to investigate the BER of the symbols detected at the receiver with the transmitted symbols. Similarly, we use the channel information estimated by different algorithms for optimal MMSE equalization, and the equalization results are shown in Fig. 6. As shown in Fig. 6, the BER performance of the OQAM-FBMC system depends on the CSI. The closer the estimated CSI is to the perfect-CSI, the better the BER performance of the system.

5.3. Suboptimal MMSE equalizer and BER

To effectively mitigate the effects of ISI, we mainly determine the number of considered symbols by normalized interference power threshold γ. Usually, γ is set artificially, and the value is taken empirically in different cases. Therefore, to quantify the ISI mitigation case, we prove that when $\gamma = 10^{-4}$, nearly all interference symbols can be considered. And the suboptimal MMSE equalization results are close to the optimal MMSE. For a fair comparison, it is necessary to guarantee that OQAM-FBMC and OFDM have the same data transmission rate. We choose the CP time spacing of OFDM to be $T_{CP} = 2.085$ μs and transmit $K = 15$ complex symbols. Therefore, the OFDM data transmission time is $K(1/F + T_{CP}) = 1.03$ ms.

Fig. 7 shows the BER performance of the suboptimal MMSE equalizer when setting different normalized interference power thresholds in a single-input single-output (SISO) system. Affected by noise and interference, a simple zero-forcing (ZF) equalizer is not effective. The suboptimal time MMSE equalization scheme [47], although improved compared to the ZF equalizer, however, fails to mitigate the effects of ISI. Fig. 8 shows that the proposed equalization scheme can be extended to MIMO systems and still achieve considerable results.

For complexity, when we consider the best results (i.e., $\gamma = 10^{-4}$, $|\zeta| = 15$), the inverse time complexity of the proposed scheme and that of optimal MMSE are shown in Table 1.

Note that the number of symbols here should be calculated according to $K = 30$. Applying such a productive equalization scheme to a MIMO transmission system can significantly

Table 1
The inverse time complexity of the optimal and suboptimal MMSE equalizers.

	SISO	MIMO[a]
Optimal MMSE	$\mathcal{O}(2.90 \times 10^{13})$	$\mathcal{O}(8.41 \times 10^{26})$
Suboptimal MMSE	$\mathcal{O}(4.15 \times 10^{8})$	$\mathcal{O}(1.72 \times 10^{17})$
Reduced volume	$\mathcal{O}(6.99 \times 10^{4})$	$\mathcal{O}(4.89 \times 10^{9})$

[a]NOTE: The complexity of the suboptimal and optimal equalizers for the MIMO system are calculated as $\mathcal{O}^2(8LK|\zeta|^3)$ and $\mathcal{O}^2(8L^3K^3)$, respectively, which can be obtained directly from the SISO formulas $\mathcal{O}(8LK|\zeta|^3)$ and $\mathcal{O}(8L^3K^3)$.

reduce the complexity of equalization at the receiver, and the equalization results are substantial.

6. Conclusion

This paper constructed a 2-D channel model for the OQAM-FBMC system and presented a pilot index stochastic optimization technique. By placing guard pilots about the effective pilot, we can mitigate the effect of ICI while channel estimation. Then, estimation performance is improved (e.g., improvement of NMSE metrics). The presented SAOSP algorithm determines the sparsity utilizing the maximum correlation lower bound value. Then, it can reconstruct the channel coefficients with a higher probability of reconstruction (e.g., improvement in reconstruction success rate). The suboptimal MMSE equalizer, based on a normalized interference power threshold, can mitigate the effects of ISI, and reduce the equalization data, thus reducing the equalization complexity (e.g., the time inverse complexity is reduced by about four orders of magnitude). Meanwhile, the equalization results are close to the optimal MMSE. However, the theoretical analyses in this paper all assume that the data are independent. The correlated data transmission and theoretical analyses still need further research.

CRediT authorship contribution statement

Ying Wang: Conceptualization, Methodology, Software. **Qiang Guo:** Investigation, Data curation. **Jianhong Xiang:** Validation, Formal analysis. **Yang Liu:** Funding acquisition.

Declaration of competing interest

The authors declare that they have no known competing financial interests or personal relationships that could have appeared to influence the work reported in this paper.

Data availability

Data will be made available on request

Acknowledgments

This work is supported in part by Fundamental Research Funds for the Central Universities, China [3072022CF0801], National Key R&D Program, China [2018YFE0206500], and Sichuan Provincial Key Laboratory of Agile Intelligent Computing Project Fund. We also thank Prof. Ronald Nissel from the Institute of Telecommunications, TU Wien for useful advice and discussion.

Appendix. Normalized interference power calculation and threshold value setting

By setting the noise to zero, the noiseless received data symbol at frequency position l and time position k can be expressed as

$$\mathbf{y}_{l,k} = ((\mathbf{Gx})^T \otimes \mathbf{g}_{l,k}^H)\text{vec}\{\mathbf{H}\}. \tag{27}$$

Where vec$\{\cdot\}$ denotes the vector generation by column. Assuming that the transmitted data are independent, we can express the interference correlation matrix $\boldsymbol{\Gamma} \in \mathbb{C}^{LK\times LK}$ as

$$\boldsymbol{\Gamma} = (\mathbf{G}^H \otimes \mathbf{g}_{l,k}^H)\mathbf{R}_H(\mathbf{G}^H \otimes \mathbf{g}_{l,k}^H)^H. \tag{28}$$

Where $\mathbf{R}_H = \text{E}\{\text{vec}\{\mathbf{H}\}\text{vec}\{\mathbf{H}\}^H\}$ denotes the channel correlation matrix. Taking $\tilde{\boldsymbol{\Gamma}} = \sqrt{\boldsymbol{\Gamma}}$ and performing phase compensation, we can obtain

$$[\boldsymbol{\Gamma}']_{i,j} = [\tilde{\boldsymbol{\Gamma}}]_{i,j}\frac{|[\tilde{\boldsymbol{\Gamma}}]_{:,j}|}{[\tilde{\boldsymbol{\Gamma}}]_{:,j}}. \tag{29}$$

Where $i, j = 1, \ldots, LK$. The interference correlation matrix after real part extraction is

$$\bar{\boldsymbol{\Gamma}} = \Re\{\boldsymbol{\Gamma}'\}\Re\{\boldsymbol{\Gamma}'\}^H. \tag{30}$$

Note that the diagonal elements of $\bar{\boldsymbol{\Gamma}} \in \mathbb{R}^{LK\times LK}$ are the interference power. In the $L \times K$ time–frequency grid, the interference power matrix $\mathbf{P}_{\text{i}} \in \mathbb{R}^{L\times K}$ can be expressed as

$$[\mathbf{P}_{\text{i}}]_{l,k} = [\text{diag}\{\bar{\boldsymbol{\Gamma}}\}]_{lk}. \tag{31}$$

Taking the parameter profile described in Section 5, the detailed value of the normalized interference power matrix $\mathbf{P}_{\text{i}}^{\text{n}} \in \mathbb{R}^{L\times K}$ is

$$\mathbf{P}_{\text{i}}^{\text{n}} = \begin{bmatrix} o(0^-) & o(0^+) & o(0^+) & o(0^+) & o(0^-) \\ o(0) & 0.0001 & 0.0002 & 0.0001 & o(0) \\ o(0^-) & 0.0002 & 0.0007 & 0.0002 & o(0^-) \\ o(0^-) & 0.0003 & 1 & 0.0002 & o(0^-) \\ o(0^-) & 0.0002 & 0.0007 & 0.0002 & o(0^-) \\ o(0) & 0.0001 & 0.0002 & 0.0001 & o(0) \\ o(0^-) & o(0^+) & o(0^+) & o(0^+) & o(0^-) \end{bmatrix}. \tag{32}$$

Where $o(0^+) \approx 1 \times 10^{-5}$, $o(0) \approx 1 \times 10^{-8}$, $o(0^-) \leq 1 \times 10^{-10}$. 1 means the reference symbol power. The matrix rows represent the frequency dimension, and the columns represent the time dimension. Therefore, the normalized interference power threshold set to $\gamma = 10^{-4}$ is sufficient to consider most of the symbol interference.

References

[1] Frank Schaich, Thorsten Wild, Rana Ahmed, Subcarrier spacing - how to make use of this degree of freedom, in: 2016 IEEE 83rd Vehicular Technology Conference (VTC Spring), 2016, pp. 1–6.
[2] Stefan Schwarz, Tal Philosof, Markus Rupp, Signal processing challenges in cellular-assisted vehicular communications: Efforts and developments within 3GPP LTE and beyond, IEEE Signal Process. Mag. 34 (2) (2017) 47–59.
[3] Stefan Schwarz, Markus Rupp, Society in motion: challenges for LTE and beyond mobile communications, IEEE Commun. Mag. 54 (5) (2016) 76–83.
[4] Anetha Mary Soman, R. Nakkeeran, Shinu Mathew John, Performance evaluation of DFT based channel estimation for spatial modulated FBMC-COQAM systems on multipath fading channels, in: 2022 IEEE International Conference on Signal Processing, Informatics, Communication and Energy Systems, Vol. 1, SPICES, 2022, pp. 123–128.
[5] Jeffrey G Andrews, Stefano Buzzi, Wan Choi, Stephen V Hanly, Angel Lozano, Anthony CK Soong, Jianzhong Charlie Zhang, What will 5G be? IEEE J. Sel. Areas Commun. 32 (6) (2014) 1065–1082.
[6] Hao Lin, Pierre Siohan, Multi-carrier modulation analysis and WCP-COQAM proposal, EURASIP J. Adv. Signal Process. 2014 (2014) 1–19.

[7] Gerhard Wunder, Peter Jung, Martin Kasparick, Thorsten Wild, Frank Schaich, Yejian Chen, Stephan Ten Brink, Ivan Gaspar, Nicola Michailow, Andreas Festag, Luciano Mendes, Nicolas Cassiau, Dimitri Ktenas, Marcin Dryjanski, Slawomir Pietrzyk, Bertalan Eged, Peter Vago, Frank Wiedmann, 5GNOW: non-orthogonal, asynchronous waveforms for future mobile applications, IEEE Commun. Mag. 52 (2) (2014) 97–105.
[8] AlaaEddin Loulou, Juha Yli-Kaakinen, Markku Renfors, Advanced low-complexity multicarrier schemes using fast-convolution processing and circular convolution decomposition, IEEE Trans. Signal Process. 67 (9) (2019) 2304–2319.
[9] Yuhao Qi, Jian Dang, Zaichen Zhang, Liang Wu, Yongpeng Wu, Efficient channel equalization and performance analysis for uplink FBMC/OQAM-Based massive MIMO systems, IEEE Trans. Veh. Technol. (2023).
[10] Samael Sarmiento, Jose A. Altabas, Salvatore Spadaro, Jose A. Lazaro, Experimental assessment of 10 gbps 5G multicarrier waveforms for high-layer split U-DWDM-PON-based fronthaul, J. Lightwave Technol. 37 (10) (2019) 2344–2351.
[11] Xiaoli Ma, G.B. Giannakis, S. Ohno, Optimal training for block transmissions over doubly selective wireless fading channels, IEEE Trans. Signal Process. 51 (5) (2003) 1351–1366.
[12] Lin Tian, Juan Li, Yi Huang, Jinglin Shi, Jihua Zhou, Seamless dual-link handover scheme in broadband wireless communication systems for high-speed rail, IEEE J. Sel. Areas Commun. 30 (4) (2012) 708–718.
[13] Khaled A. Alaghbari, Heng-Siong Lim, Tawfig Eltaif, Benzhou Jin, Lian Hong Lee, Filterbank-assisted channel estimation for coherent optical FBMC/OQAM system, IEEE Photonics J. 14 (6) (2022) 1–7.
[14] Taehyun Lee, Dongkyu Sim, Bongsung Seo, Chungyong Lee, Channel estimation scheme in oversampled frequency domain for FBMC-QAM systems based on prototype filter set, IEEE Trans. Veh. Technol. 68 (1) (2019) 728–739.
[15] Wenfeng Liu, Stefan Schwarz, Markus Rupp, Da Chen, Tao Jiang, Preamble-based channel estimation for OQAM/FBMC systems with delay diversity, IEEE Trans. Wireless Commun. 19 (11) (2020) 7169–7180.
[16] Mario Tanda, Performance analysis of FBMC/OQAM systems in frequency-selective channels, Digit. Signal Process. 134 (2023) 103935.
[17] Seyed Mahmoud Pishvaei, Behzad Mozaffari Tazehkand, Jafar Pourrostam, Design and performance evaluation of FBMC-based orthogonal time–frequency space (OTFS) system, Phys. Commun. 53 (2022) 101723.
[18] Walid A. Raslan, Mohamed A. Mohamed, Heba M. Abdel-Atty, Deep-BiGRU based channel estimation scheme for MIMO–FBMC systems, Phys. Commun. 51 (2022) 101592.
[19] Eleftherios Kofidis, Dimitrios Katselis, Athanasios Rontogiannis, Sergios Theodoridis, Preamble-based channel estimation in OFDM/OQAM systems: A review, Signal Process. 93 (7) (2013) 2038–2054.
[20] Da Chen, Rui Wang, Tao Jiang, Channel estimation and pilot symbol optimization based on intrinsic interference utilization for OQAM/FBMC systems, IEEE Trans. Signal Process. 69 (2021) 4595–4606.
[21] Jamal Bazzi, Petra Weitkemper, Katsutoshi Kusume, Power efficient scattered pilot channel estimation for FBMC/OQAM, in: SCC 2015; 10th International ITG Conference on Systems, Communications and Coding, 2015, pp. 1–6.
[22] Wenjia Cui, Daiming Qu, Tao Jiang, Behrouz Farhang-Boroujeny, Coded auxiliary pilots for channel estimation in FBMC-OQAM systems, IEEE Trans. Veh. Technol. 65 (5) (2016) 2936–2946.
[23] Ronald Nissel, Fjolla Ademaj, Markus Rupp, Doubly-selective channel estimation in FBMC-OQAM and OFDM systems, in: 2018 IEEE 88th Vehicular Technology Conference (VTC-Fall), 2018, pp. 1–5.
[24] Zongmiao He, Lingyu Zhou, Yang Yang, Yiou Chen, Xiang Ling, Changjian Liu, Compressive sensing-based channel estimation for FBMC-OQAM system under doubly selective channels, IEEE Access 7 (2019) 51150–51158.
[25] Defeng Ren, Jing Li, Guangyue Lu, Jianhua Ge, Joint channel estimation and equalization using new AFB output signal models for FBMC/OQAM systems, IEEE Trans. Commun. 69 (6) (2021) 4186–4201.
[26] Prem Singh, Suraj Srivastava, Amrita Mishra, Aditya K. Jagannatham, Lajos Hanzo, Sparse Bayesian learning aided estimation of doubly-selective MIMO channels for filter bank multicarrier systems, IEEE Trans. Commun. 70 (6) (2022) 4236–4249.
[27] Maurice Bellanger, FS-FBMC: An alternative scheme for filter bank based multicarrier transmission, in: 2012 5th International Symposium on Communications, Control and Signal Processing, 2012, pp. 1–4.
[28] Màrius Caus, Ana I. Perez-Neira, Transmitter-receiver designs for highly frequency selective channels in MIMO FBMC systems, IEEE Trans. Signal Process. 60 (12) (2012) 6519–6532.
[29] Dirk S. Waldhauser, Leonardo G. Baltar, Josef A. Nossek, MMSE subcarrier equalization for filter bank based multicarrier systems, in: 2008 IEEE 9th Workshop on Signal Processing Advances in Wireless Communications, 2008, pp. 525–529.
[30] Ronald Nissel, Markus Rupp, Roman Marsalek, FBMC-OQAM in doubly-selective channels: A new perspective on MMSE equalization, in: 2017 IEEE 18th International Workshop on Signal Processing Advances in Wireless Communications, SPAWC, 2017, pp. 1–5.
[31] Davide Mattera, Mario Tanda, Maurice Bellanger, On single-tap equalization for an FBMC multicarrier system in wireless channels, Signal Process. 194 (2022) 108434.
[32] Husam Al-Amaireh, Zsolt Kollár, Low complexity PPN-FBMC receivers with improved sliding window equalizers, Phys. Commun. 54 (2022) 101795.
[33] Ahmad Rezazadeh Reyhani, Behrouz Farhang-Boroujeny, An analytical study of circularly pulse-shaped FBMC-OQAM waveforms, IEEE Signal Process. Lett. 24 (10) (2017) 1503–1506.
[34] Bernard Le Floch, Michel Alard, Claude Berrou, Coded orthogonal frequency division multiplex [TV broadcasting], Proc. IEEE 83 (6) (1995) 982–996.
[35] Maurice Bellanger, D. Le Ruyet, D. Roviras, M. Terré, J Nossek, L Baltar, Q Bai, D Waldhauser, M Renfors, T Ihalainen, et al., FBMC physical layer: a primer, PHYDYAS, January 25 (4) (2010) 7–10.
[36] Georg Taubock, Franz Hlawatsch, A compressed sensing technique for OFDM channel estimation in mobile environments: Exploiting channel sparsity for reducing pilots, in: 2008 IEEE International Conference on Acoustics, Speech and Signal Processing, 2008, pp. 2885–2888.
[37] G.B. Giannakis, C. Tepedelenlioglu, Basis expansion models and diversity techniques for blind identification and equalization of time-varying channels, Proc. IEEE 86 (10) (1998) 1969–1986.
[38] Peng Cheng, Zhuo Chen, Yun Rui, Y. Jay Guo, Lin Gui, Meixia Tao, Q.T. Zhang, Channel estimation for OFDM systems over doubly selective channels: A distributed compressive sensing based approach, IEEE Trans. Commun. 61 (10) (2013) 4173–4185.
[39] Dongjun Na, Kwonhue Choi, Low PAPR FBMC, IEEE Trans. Wireless Commun. 17 (1) (2018) 182–193.
[40] Marco F. Duarte, Yonina C. Eldar, Structured compressed sensing: From theory to applications, IEEE Trans. Signal Process. 59 (9) (2011) 4053–4085.
[41] Wei Dai, Olgica Milenkovic, Subspace pursuit for compressive sensing signal reconstruction, IEEE Trans. Inform. Theory 55 (5) (2009) 2230–2249.
[42] Joel A. Tropp, Anna C. Gilbert, Signal recovery from random measurements via orthogonal matching pursuit, IEEE Trans. Inform. Theory 53 (12) (2007) 4655–4666.
[43] Muhammad Sajjad, Irfan Mehmood, Sung Wook Baik, Sparse coded image super-resolution using K-SVD trained dictionary based on regularized orthogonal matching pursuit, Bio-Med. Mater. Eng. 26 (s1) (2015) S1399–S1407.
[44] Abolfazl Hashemi, Haris Vikalo, Sparse linear regression via generalized orthogonal least-squares, in: 2016 IEEE Global Conference on Signal and Information Processing (GlobalSIP), 2016, pp. 1305–1309.
[45] Menghang Wu, Feiyun Wu, Kunde Yang, Tian Tian, A multipath matching pursuit algorithm based on improved-inner product matching criterion, in: 2020 IEEE International Conference on Signal Processing, Communications and Computing, ICSPCC, 2020, pp. 1–5.
[46] Mojisola Grace Asogbon, Yu Lu, Oluwarotimi Williams Samuel, Liwen Jing, Alice A. Miller, Guanglin Li, Kelvin K.L. Wong, GBRAMP: A generalized backtracking regularized adaptive matching pursuit algorithm for signal reconstruction, Comput. Electr. Eng. 92 (2021) 107189.
[47] Ljiljana Marijanović, Stefan Schwarz, Markus Rupp, MMSE equalization for FBMC transmission over doubly-selective channels, in: 2016 International Symposium on Wireless Communication Systems, ISWCS, 2016, pp. 170–174.

Ying Wang received the B.S. degree in Communication Engineering from Henan College of Engineering in 2021. He is currently pursuing a Ph.D. in Information and Communication Engineering at Harbin Engineering University. His research interests are in signal processing, 5G/6G wireless communications, orthogonal modulation schemes (e.g., OFDM), non-orthogonal modulation schemes (e.g., FBMC), massive MIMO, etc.

Qiang Guo received the M.S. and Ph.D. degrees from Harbin Engineering University in 2003 and 2007, respectively. He is an expert in degree and postgraduate education accreditation at the Chinese Education Ministry and a Foreign Member of the Ukraine Academy of Engineering. Currently, He is working as the Ocean-Revival Academic Team leader of Harbin Engineering University on "Communication System and Technology in Complex Electromagnetic Environment." His research interests are radar detection and countermeasures, 5G/6G wireless communications, and satellite communications.

Jianhong Xiang received M.S. and Ph.D. degrees from Harbin Engineering University in 2006 and 2009, respectively. He is the Deputy Director of the Ships Communication and Countermeasures Technology Institute. Currently, He is working as the Ocean-Revival Academic Team Membership of Harbin Engineering University on "Communication System and Technology in Complex Electromagnetic Environment." His research interests include "intelligent signal processing," 5G/6G wireless communication, artificial intelligence, and communication countermeasures.

Yang Liu received the Ph.D. degree in Signal and Information Processing from Southwest Jiaotong University in 2014. Since 2019, he has been working as a Senior Engineer at CLP 10 Research Institute. His recent research focus is on 5G/6G wireless transmission and waveform optimization.